Electrochimica Acta 485 (2024) 144084

Contents lists available at ScienceDirect

Electrochimica Acta

journal homepage: www.journals.elsevier.com/electrochimica-acta

# Electrolyte design for the manipulation of gas bubble detachment during hydrogen evolution reaction

Sunghak Park [a,b,*], Detlef Lohse [c,d], Dominik Krug [c], Marc T.M. Koper [a,*]

[a] Leiden Institute of Chemistry, Leiden University, Leiden, the Netherlands
[b] Department of Future Energy Engineering and Sungkyunkwan University Institute of Energy Science & Technology (SIEST), Sungkyunkwan University, Suwon, Gyeonggi-do 16419, Republic of Korea
[c] Physics of Fluids Group, Max Planck Center Twente for Complex Fluid Dynamics, Faculty of Science and Technology, University of Twente, Enschede, the Netherlands
[d] Max Planck Institute for Dynamics and Self-Organization, Göttingen, Germany

ARTICLE INFO

*Keywords:*
$H_2$ gas bubble detachment
Microbubbles coalescence
Thermal Marangoni effect
Solutal Marangoni effect

ABSTRACT

During electrochemical gas evolution reactions, the continuous and vigorous formation of gas bubbles hugely impacts the efficiency of the underlying electrochemical processes. In particular, enhancing the detachment of gas bubbles from the electrode surface has emerged as an effective strategy to improve reaction efficiency. In this study, we demonstrate that the detachment of $H_2$ gas bubbles can be controlled by the electrolyte composition, which can be optimized. We employ a well-defined Pt microelectrode and utilize electrochemical oscillation analysis to elucidate the features of $H_2$ gas bubble detachment. Our investigation explores how the behaviour of $H_2$ gas bubbles responds to variations in electrolyte composition and concentration. The coalescence efficiency of electrochemically generated microbubbles, a critical factor determining the mode of $H_2$ gas bubble detachment (random detachment vs. single $H_2$ gas bubble detachment), is profoundly influenced by the electrolyte composition. Specifically, coalescence efficiency follows the Hofmeister series concerning anions and coalescence is consistently inhibited in the presence of alkali metal cations. Furthermore, we establish a comprehensive model that accounts for both thermal and solutal Marangoni effects, allowing us to rationalize the trend of detachment size and period of single $H_2$ gas bubbles under various conditions.

## 1. Introduction

The production of green hydrogen via water electrolysis, powered by renewable electricity, is receiving increasing attention in the context of achieving the energy transition, particularly in situations where direct electrification is not feasible [1–3]. During water electrolysis, hydrogen and oxygen gases are continuously generated at the cathode and anode, respectively [4,5]. The limited solubility and diffusivity of these gaseous products in aqueous solution [6,7] result in a notable supersaturation level close to the electrode. Consequently, the formation and evolution of gas bubbles, including their nucleation, growth, coalescence, and detachment from the electrode, are inevitable phenomena during high-current density water electrolysis. Therefore, a comprehensive understanding of gas bubble behaviour is pivotal for optimizing the efficiency of water electrolysis [8,9].

Extensive studies have shown that the evolution of gas bubbles profoundly influences various aspects of electrochemical processes: reducing the active surface area due to adherent bubbles [10,11], changing the gas concentration and electric field profile [12,13], increasing solution ohmic resistance [14], modifying mass transport due to convective flow resulting from the growth and detachment of gas bubbles [15], and so on. Although a detailed understanding of the intricate interdependencies between gas bubble evolution, transport and their impact on water electrolyser performance remains elusive, it has been reported that approaches enhancing the facile elimination of gas bubbles from the electrode surface lead to noticeable improvements in device performance [16,17]. Hence, it is of particular importance to gain insights into the fundamental gas bubble detachment processes occurring on the electrode surface under electrochemical conditions.

One of the simplest models employed to understand gas bubble detachment from the solid surface is known as the Fritz model, which determines the detachment size of the growing gas bubble with a spreading contact line by considering the balance between capillarity and buoyancy [18]. However, experimental observations reveal that the

* Corresponding authors.
*E-mail addresses:* s.park@lic.leidenuniv.nl, sunghak@skku.edu (S. Park), m.koper@lic.leidenuniv.nl (M.T.M. Koper).

https://doi.org/10.1016/j.electacta.2024.144084
Received 14 December 2023; Received in revised form 17 February 2024; Accepted 9 March 2024
Available online 10 March 2024

gas bubble detachment size during electrochemical or other gas-evolving reactions is generally smaller than the estimated values derived from the simple Fritz model [19,20]. This discrepancy might be attributed to factors such as contact line pinning [19], bubble coalescence-induced detachment [21,22], and other contributing forces. In the case of electrochemically generated gas bubbles, Lubetkin suggested two additional forces to be considered [23,24]: 1) the electrostatic force arising from an excess charge at bubble/electrolyte interface with the polarized electrode, and 2) the Marangoni force originating from the surface tension gradient along the bubble/electrolyte interface due to concentration and/or temperature gradients occurring during the electrochemical reaction. The group of Eckert has experimentally validated the significance of these contributing factors in the case of single $H_2$ gas bubble detachment on a 100 μm Pt microelectrode in $H_2SO_4$ [25,26]. In particular, they proposed a significant role of the thermal Marangoni effect on single $H_2$ gas bubble detachment under their experimental conditions, which is induced by a temperature gradient due to severe ohmic heating [27], and they proposed a physical force balance model that accounts for both contributions [28]. This experimentally observed Marangoni convection can be better predicted with numerical simulations that consider the stagnant cap on the bubble interface, which might be attributed to possible contaminants [29]. Recently, our groups reported that the type of anion in acid electrolytes have a critical impact on $H_2$ gas bubble detachment [30]. This phenomenon arises from differences in the coalescence efficiency of electrochemically generated microbubbles, following the Hofmeister series of anions. Moreover, the detachment size of a single $H_2$ gas bubble is strongly influenced by solutal Marangoni effects, driven by ion concentration gradients along the bubble/electrolyte interface.

In this work, we aim to expand upon our previous findings by encompassing a multitude of electrolyte conditions and their impact in $H_2$ gas bubble detachment, and presenting new possibilities for bubble management through electrolyte "design"-i.e., by optimizing the composition and concentration of the electrolytes. To achieve this, we study $H_2$ gas bubble behaviour by analyzing the electrochemical oscillation at a 100 μm Pt microelectrode under various electrolyte compositions and concentrations. Our observations indicate that the coalescence efficiency of electrochemically generated $H_2$ microbubbles can be effectively controlled by modifying the electrolyte composition. The coalescence efficiency follows the Hofmeister series of anions in all acidic electrolytes we studied. The addition of alkali metal cations to the electrolyte reduces microbubble coalescence efficiency, regardless of the type of anion. Consequently, multiple $H_2$ microbubbles detach randomly in neutral and alkaline electrolytes containing a substantial amount of alkali metal cations, in contrast to periodic formation and detachment of single $H_2$ gas bubbles observed in some acid electrolytes. We also elucidate the electrolyte-dependent detachment of single $H_2$ gas bubbles by considering the interplay of the two different Marangoni effects (solutal and thermal) across all the studied electrolyte conditions. We believe these findings provide valuable insights for the design of electrolytes for $H_2$ gas bubble manipulation.

## 2. Experimental

### 2.1. Chemicals

All chemicals were used without further purification process. The electrolytes were prepared from $H_2SO_4$ (96 %, Suprapur, Merck), HCl (30 %, Suprapur, Merck), $HNO_3$ (65 %, Suprapur, Merck), $HClO_4$ (60 %, EMSURE, Merck), $H_3PO_4$ (85 %, Suprapur, Merck), $CH_3COOH$ (99.8 %, Suprapur, Merck), $Li_2SO_4{\cdot}xH_2O$ (99.99 %, Merck), $Na_2SO_4$ (99.99 %, Alfa Aesar), $K_2SO_4$ (99.997 %, Alfa Aesar), $Cs_2SO_4$ (99.99 %, Alfa Aesar), $NaClO_4{\cdot}xH_2O$ (99.99 %, Merck), NaOH solution (30 %, Suprapur, Merck), and Milli-Q water (≥18.2 MΩ cm, TOC < 5 ppb).

### 2.2. Microelectrode preparation

The Pt microelectrode was fabricated by sealing a Pt wire (100 μm diameter, 99.99 %, Goodfellow) within a soda-lime glass capillary (1.4 mm outer diameter, 1.12 mm inner diameter, Hilgenberg) using a butane torch. The prepared Pt microelectrode underwent mechanical polishing with diamond polishing suspension of decreasing particle size (3.0, 1.0, 0.25, 0.05 μm, Buehler) on micropolishing cloth, followed by sandpaper polishing (P2000, Starcke). Between each polishing step, the Pt microelectrode was sonicated in Milli-Q water for 10 min to remove any residual debris. Finally, the Pt microelectrode surface was cleaned through oxidation–reduction cycling between 0.03 and 1.35 $V_{RHE}$ (30 times, 1 V $s^{-1}$) in Ar purged $H_2SO_4$.

### 2.3. Electrochemical characterization

The electrochemical characterization was conducted using a homemade PEEK cell equipped with a transparent glass window on the side. The electrochemical cell was placed in a permanganate solution overnight (0.5 M $H_2SO_4$, 1 g $L^{-1}$ $KMnO_4$). Prior to usage, the cell was rinsed and submerged in a diluted piranha solution to remove any residual $MnO_2$, followed by multiple rinsing and boiling with Milli-Q water. Linear sweep voltammetry and chronoamperometry measurements were performed using a three-electrode configuration with a Bio-Logic SP300 potentiostat. A platinum wire (99.9 %, MaTeck) and leakless Ag/AgCl (ET072–1, eDAQ) were used as counter and reference electrode, respectively. The surface of Pt microelectrode was oriented upwards to study freely detachable $H_2$ gas bubble behaviours. Before each measurement, the electrolyte was purged with Ar bubbling for 10 min to remove $O_2$, and this Ar purging was discontinued throughout the measurements. The evolution of $H_2$ gas bubbles on the microelectrode was recorded using a digital microscope (USB Microscope 5 MP, Toolcraft).

### 2.4. Electrochemical oscillation analysis

The period was determined by analysing the time between consecutive peak points of electrochemical oscillation. The estimated detachment radius ($R_D$) was calculated using the following equation:

$$R_D = \left[\frac{-3RTQ}{8\pi FP_0}\right]^{1/3}$$

where $R$, $T$, $Q$, $F$, and $P_0$ are the gas constant, the temperature, the current integrated over one oscillation period, the Faraday constant, and the atmospheric pressure, respectively. It is important to note that our calculation assumes that all of the produced $H_2$ gas is captured by a single $H_2$ gas bubble, which has been validated by previous studies [30,31].

## 3. Results

### 3.1. Electrochemical oscillation and $H_2$ gas bubble behaviours in various acid electrolytes

To obtain a comprehensive overview of $H_2$ gas bubble behaviour in various acidic electrolytes, we investigated electrochemical oscillations during linear sweep voltammetry (LSV) in six different acidic electrolytes. A scan rate of 100 mV $s^{-1}$ was employed, which is slow enough to capture the oscillatory features at different potentials (see Fig. 1). In the case of the four strong acids (Fig. 1a-1d and Supplementary Figure 1), the observed oscillating features were in good agreement with previous findings obtained through chronoamperometry measurements [30]. To explain anion-dependent $H_2$ gas bubble behaviour during hydrogen evolution reaction (HER), we proposed a model considering microbubble coalescence and the Marangoni effect: 1) The onset of periodic oscillation, signifying the periodic formation and detachment of single

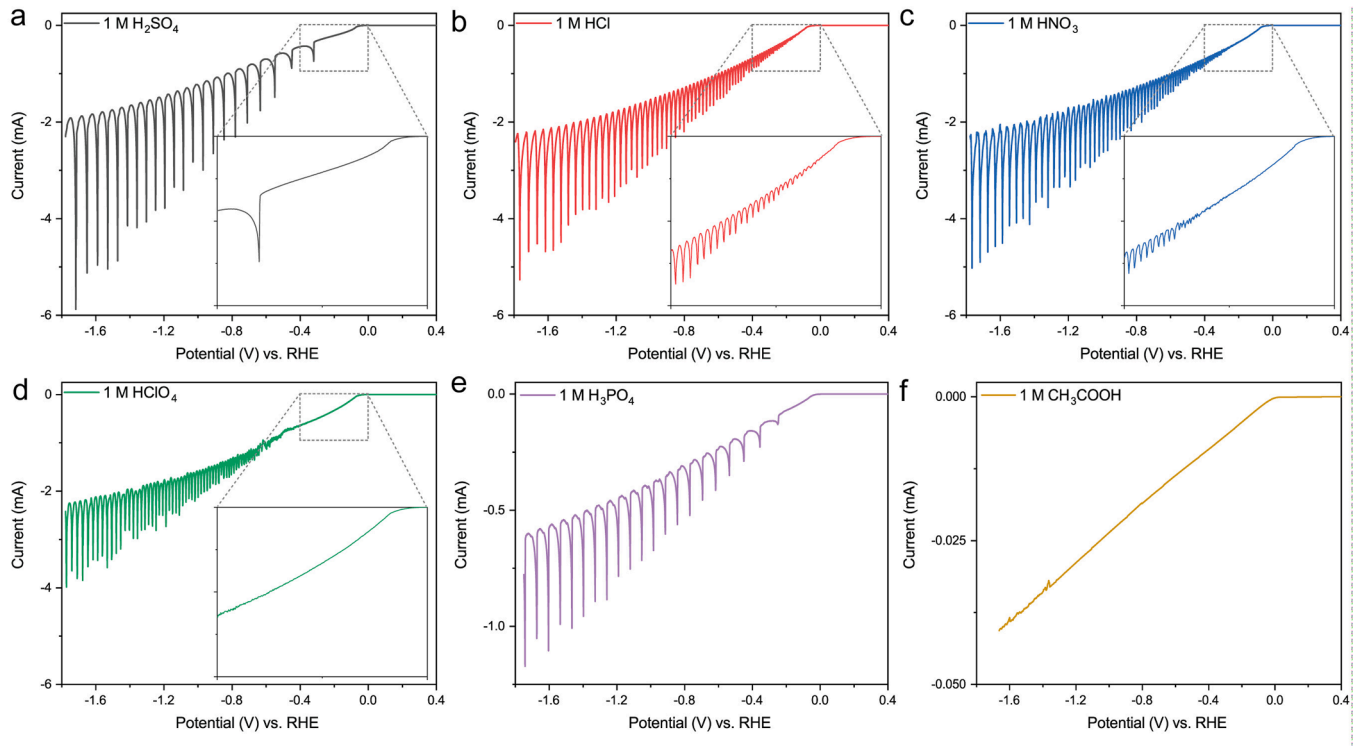


**Fig. 1.** Anion effects on $H_2$ gas bubble behaviour in acid electrolytes. Linear sweep voltammetry (LSV) of Pt microelectrode in different electrolytes: 1 M $H_2SO_4$ (a), HCl (b), $HNO_3$ (c), $HClO_4$ (d), $H_3PO_4$ (e), and $CH_3COOH$ (f). Scan rate: 100 mV $s^{-1}$. The insets in Fig. 1a-1d show enlarged graphs of the low overpotential region from 0 to –0.4 $V_{RHE}$, enclosed in gray dotted boxes.

$H_2$ gas bubbles, follows the Hofmeister series of anions. This phenomenon arises from variations in the coalescence efficiency of microbubbles for different anions. 2) The sequence of oscillation periods, which reflects the detachment period of a single $H_2$ gas bubble, correlates with the surface tension increment ($\sigma_C \equiv \partial\Delta\sigma/\partial C$) values for different electrolytes ($H_2SO_4$: 0.44 > HCl: –0.27 > $HNO_3$: –0.83 > $HClO_4$: –2.15, unit: $mN\ m^{-1}/mol\ L^{-1}$) [32]. We explained this correlation by different solutal Marangoni effects for different electrolytes. The necessary anion concentration gradient to induce this solutal Marangoni effect, is related to the proton concentration gradient that exists during high-rate hydrogen evolution. Due to the need to satisfy electroneutrality, this proton concentration gradient is matched by a corresponding anion concentration gradient. Specifically, a larger positive value of $\sigma_C$ of the electrolyte leads to a larger electrode-directed Marangoni force, promoting bubble coalescence and a larger oscillation period; on the other hand, a negative $\sigma_C$ gives a reverse-directed solutal Marangoni effect, facilitating gas bubble detachment. Largely independent of the electrolyte identity, there is also a thermal Marangoni effect, which leads to electrode-directed Marangoni effect, especially at (very) high current density.

We extended our investigation to include two additional acid electrolytes, $H_3PO_4$ and $CH_3COOH$, classified as weak acids with larger pKa values [33]. The solution of 1 M $H_3PO_4$ has a measured bulk pH of 1.10. As the overpotential increases, the HER current level rises, and we observe periodic current oscillations across the entire potential range (Fig. 1e). The shape and the period of the oscillation exhibit similar features to that of 1 M $H_2SO_4$ (Fig. 1e and Supplementary Figure 1), although the absolute current is lower due to the lower effective pH. The periodic oscillation across the wide potential window can be rationalized by the high coalescence efficiency of microbubbles in 1 M $H_3PO_4$, taking into consideration that phosphate anions lie close to sulfate anions in the Hofmeister series [34]. Compared to 1 M $H_2SO_4$, a faster detachment period for single $H_2$ gas bubbles is observed in 1 M $H_3PO_4$ under the same average current conditions (Supplementary Figure 1), suggesting a smaller solutal Marangoni force in 1 M $H_3PO_4$. Although similar ion concentration gradients are expected for both electrolytes under given current conditions, the surface tension gradient can differ due to differences in $\sigma_C$. It should be noted that 1 M $H_3PO_4$ contains a large number of undissociated $H_3PO_4$ molecules, along with protons and (partially) dissociated phosphate anions, due to less than 10 % dissociation of $H_3PO_4$ molecules [35]. While the $\sigma_C$ of $H_3PO_4$ is reported to be 0.85 $mN\ m^{-1}/mol\ L^{-1}$ [32], the exact contributions from ions versus undissociated $H_3PO_4$ are not clearly defined. In this context, one plausible explanation for our observation is that the surface tension changes driven by (partially) dissociated phosphate anions are less pronounced than those caused by sulfate anions. Nevertheless, further investigation is required to fully elucidate the surface tension gradient in $H_3PO_4$.

It is noteworthy that the LSV curve shapes of 1 M $H_3PO_4$ and 50 mM $H_2SO_4$ (Supplementary Figure 2) are different, despite their similar bulk pH levels. In 50 mM $H_2SO_4$, the LSV curve exhibits a plateau current region, which arises from proton transport limitation (more discussion on experiments in dilute $H_2SO_4$ will follow later). In contrast, the LSV curve for 1 M $H_3PO_4$ shows a linear increase in HER current without a proton transport-limited region, indicating that both undissociated and partially-dissociated phosphates, as well as free protons, serve as proton donors during the reaction [36].

As for 1 M $CH_3COOH$, the observed LSV curve displays a much lower HER current within the same potential window compared to other acid electrolytes due to its high pH (2.35). At a potential of –1.06 $V_{RHE}$, we observed the detachment of very small-sized $H_2$ gas bubbles, approximately 20 μm in size, which does not lead to a periodically oscillating HER current due to the small size of $H_2$ gas bubbles compared to the electrode dimension of 100 μm (Supplementary Figure 3). Upon lowering the applied potential to –1.66 $V_{RHE}$, a small fluctuating HER current was observed corresponding with random detachment of multiple microbubbles (Supplementary Figure 3). From these observations, we conclude that there is a pronounced coalescence suppression in 1 M $CH_3COOH$ across the entire potential window investigated.

To gain further insight into the manipulation of single $H_2$ gas bubble detachment, we conducted a study on electrochemical oscillation while adjusting the concentration of $H_2SO_4$, the electrolyte which showed the highest microbubble coalescence efficiency among the acidic electrolytes we previously tested [30]. In Fig. 2a, we present LSV curves obtained from 1, 0.5, 0.25 M $H_2SO_4$ electrolytes, all of which exhibit similar oscillating features. The electrochemical oscillation of the HER current is observable across the entire HER potential window that we measured. With decreasing concentration of $H_2SO_4$, both the HER current level and the amplitude of oscillation decreases, attributed to the lower proton concentration. From the oscillation period, we derived the detachment period of a single $H_2$ gas bubble (Fig. 2b and Supplementary Figure 4). Overall, graphs plotting the oscillation period vs. average current (or potential) exhibit v-shaped curves for all $H_2SO_4$ concentrations, in good agreement with previous results in 1 M $H_2SO_4$ [30]. In Fig. 2b, we plotted the period vs. the average current per oscillation rather than the applied potential, because of the substantial differences in HER current level for different $H_2SO_4$ concentrations.

In our previous study [30], we rationalized the v-shaped period-potential or period-current curve in 1 M $H_2SO_4$ by considering the two different Marangoni effects, i.e. thermal and solutal, as expressed by:

$$F_{Mar} \propto \Delta\sigma = \sigma_C \frac{\partial C}{\partial s} L_C + \sigma_T \frac{\partial T}{\partial s} L_T \approx \sigma_C \frac{\Delta C}{L_C} L_C + \sigma_T \frac{\Delta T}{L_T} L_T = \sigma_C \Delta C + \sigma_T \Delta T \quad (1)$$

In this equation, $F_{Mar}$, $\Delta\sigma$, $\sigma_X$, $s$ and $L_X$ denote the force on single $H_2$ gas bubble due to the Marangoni effect, the surface tension change along the gas bubble/electrolyte interface, the partial derivative of surface tension with respect to $X$ (where $X$ can be (anion) concentration, $C$, or temperature, $T$), the tangential coordinate along the gas bubble/electrolyte interface, and the characteristic length scale of the gradient field of $X$, respectively. Based on this model, the $\sigma_C \Delta C$ term (solutal Marangoni effect) dominates at the low HER current region, while at the high HER current region, the $\sigma_T \Delta T$ term (thermal Marangoni effect) becomes dominant due to ohmic heating (Fig. 3). The temperature change ($\Delta T$) can be estimated by $\Delta T = -\frac{l^2}{k\kappa_{el}A^2} I^2 \propto I^2$, where $k$ represents the thermal conductivity, $\kappa_{el}$ represents the electrical conductivity, $I$ is the average current per oscillation, and $A$ and $l$ are the area and length of the heat transfer path, determined by the geometric configuration of the electrochemical system (see Supplementary Note 1 for more discussion). The value of $I_{trans}$ ($I$ at the transition point), where these two competing factors are comparable, can be estimated from the minimum of v-shaped

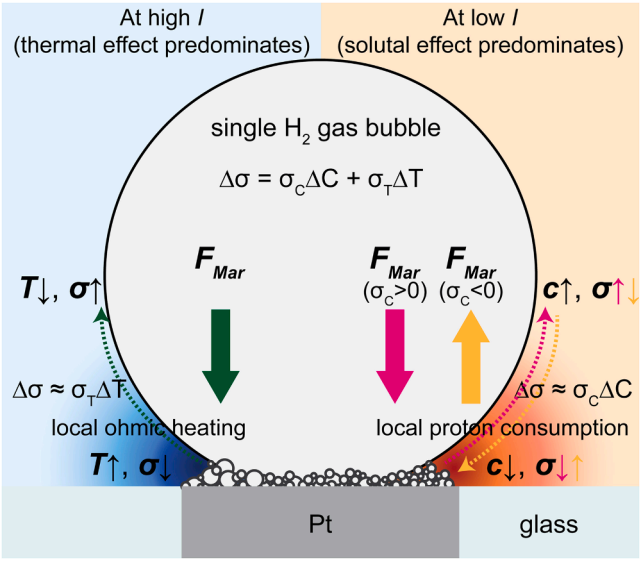


**Fig. 3.** Schematic illustration of the proposed dual Marangoni effects mechanism. The illustration shows surface tension gradients influenced by two factors: on the left, a temperature gradient induced by local ohmic heating (representing the thermal Marangoni effect); on the right, an ion concentration gradient resulting from local proton consumption (representing the solutal Marangoni effect). For all aqueous electrolytes we studied, the thermal Marangoni force is directed towards the electrode. Conversely, the direction of the solutal Marangoni force depends on the characteristics of electrolyte: it is directed towards the electrode in electrolytes with a $\sigma_C > 0$, and away from the electrode in electrolytes with a $\sigma_C < 0$.

period-current curve. Note that we expect the $\sigma_C \Delta C$ term to be linear in $I$, as the concentration gradient scales linearly with $I$, and that the $\sigma_T \Delta T$ term scales quadratically with $I$ (see Supplementary Note 2 for more discussion).

As shown in Fig. 2b, the values of $I_{trans}$ decrease with a decrease in $H_2SO_4$ concentration. At a given average current condition, a lower $H_2SO_4$ concentration reduces the relative contribution of the solutal Marangoni effect due to the decreased $\Delta C$. Conversely, the relative contribution of the thermal Marangoni effect increases due to the increased $\Delta T$, originating from stronger ohmic heating caused by decreased $\kappa_{el}$. This leads to a shift in the transition point where the solutal and thermal effects are equal in magnitude, i.e. toward a smaller

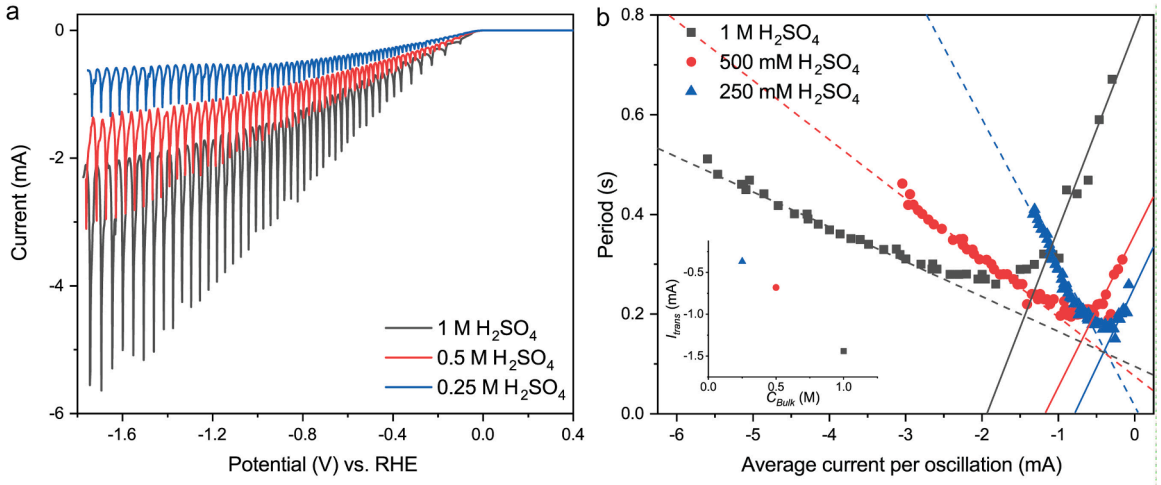


**Fig. 2.** $H_2SO_4$ concentration effects on periodic formation and detachment of single $H_2$ gas bubble. a, LSV curves with a scan rate of 100 mV $s^{-1}$. b, Period of oscillation versus the average current per oscillation. Solid and dotted lines serve as guidelines for the conditions where the solutal and thermal Marangoni effects are dominant, respectively. Inset graphs show $I_{trans}$ values obtained from different $H_2SO_4$ concentrations.

$I_{trans}$ with decreasing $H_2SO_4$ concentration. To gain a more quantitative perspective, we consider using the upper limit value of $\Delta C \sim C_{Bulk}$, which aligns with the rapid proton consumption at high current densities during the experiments (geometric current density of –6.4 A $cm^{-2}$ at –0.5 mA). Then, $I_{trans}$ and $C_{Bulk}$ are related via

$$1 = \frac{\sigma_C \Delta C(I = I_{trans})}{\sigma_T \Delta T(I = I_{trans})} \approx \frac{\sigma_C C_{Bulk}}{-\sigma_T l^2 {I_{trans}}^2 / k\kappa_{el} A^2} = \frac{\sigma_C C_{Bulk}}{-\sigma_T l^2 {I_{trans}}^2 / k\Lambda_m C_{Bulk} A^2}$$
$$= \frac{\sigma_C k \Lambda_m {C_{Bulk}}^2 A^2}{-\sigma_T l^2 {I_{trans}}^2} \quad (2)$$

where $\Lambda_m$ is the molar conductivity of $H_2SO_4$. Assuming a constant $\Lambda_m$, the magnitude of $I_{trans}$ is proportional to $C_{Bulk}$, which is confirmed by the results obtained for the three different concentrations: values of $I_{trans}$ are –1.44, –0.68 and –0.37 mA at 1 M, 500 mM, 250 mM $H_2SO_4$, respectively.

In 100 mM $H_2SO_4$, the LSV curve exhibits a sigmoidal shape with electrochemical oscillations across the entire potential window, as shown in Fig. 4a. As the overpotential increases, the HER current initially rises, and from –0.6 $V_{RHE}$, a plateau region is observed where the HER current oscillates between –0.15 and –0.26 mA. This plateau corresponds to the mass transport limited proton reduction. On the other hand, in the case of 1 M $H_3PO_4$, which has a higher pH value (indicating a lower bulk proton concentration), the HER current level increases monotonously with overpotential (see Fig. 1e) without any plateau region up to –1 mA (corresponding to –12.7 A $cm^{-2}$ of geometric current density). Both electrolytes exhibit a periodically oscillating HER current, indicating the periodic formation and detachment of single $H_2$ gas bubbles. Assuming a similar pattern of convective flow induced by the single $H_2$ gas bubble detachment in both electrolytes, we attribute the difference in LSV curve shape to the different amounts of undissociated/partially-dissociated electrolytes, which can serve as an additional proton source for HER [36]. In 1 M $H_3PO_4$, the high concentration of undissociated/partially-dissociated (hydrogen)phosphates provides enough additional protons up to –1 mA, while, in the plateau region of 100 mM $H_2SO_4$, proton transport is limiting. The HER current level in 100 mM $H_2SO_4$ starts to increases again from around –1.6 $V_{RHE}$, which we assign to water reduction, since the only remaining available proton donor in this system is water. This assignment is further supported by an increase in the HER current in the region below –1.6 $V_{RHE}$ upon the

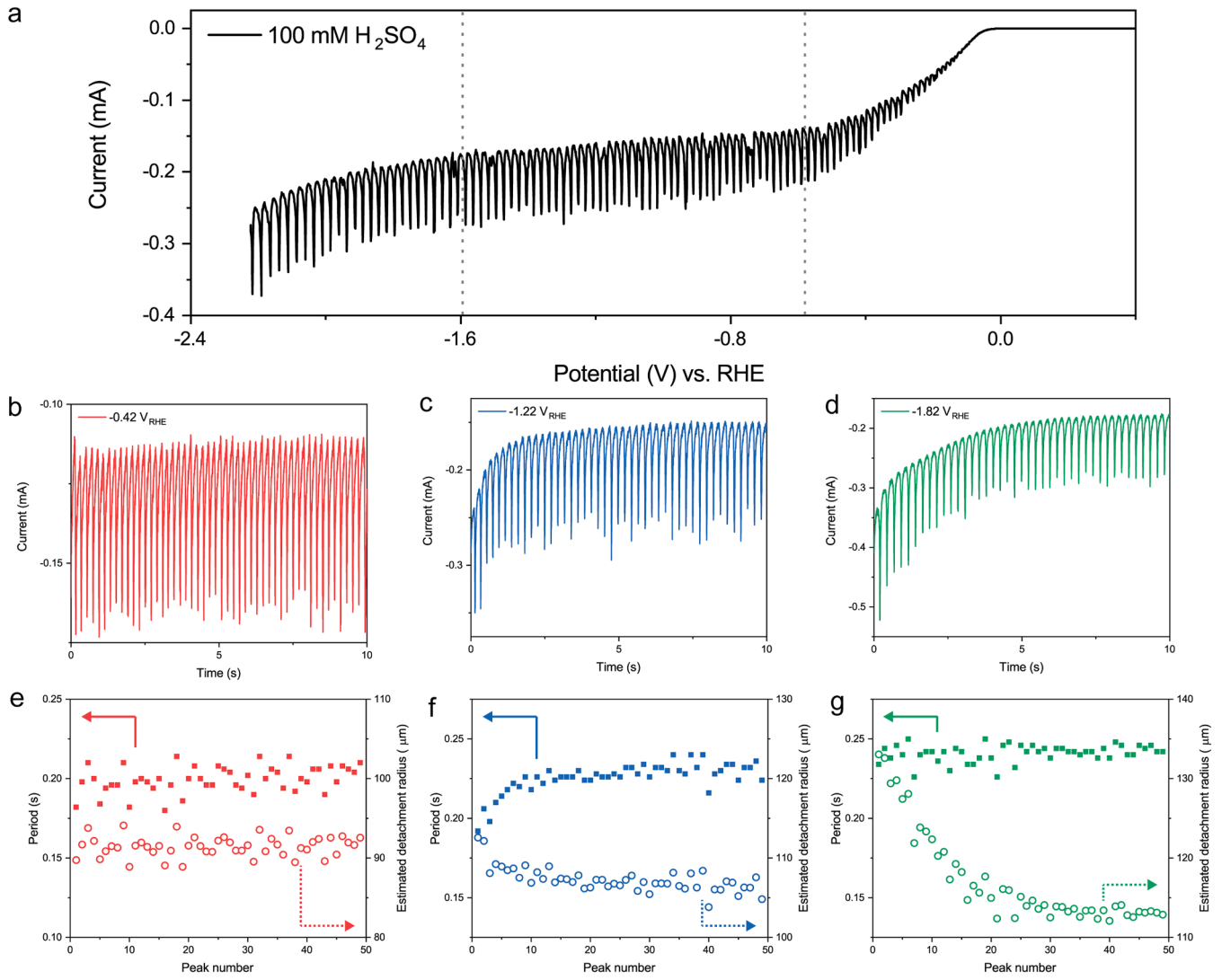


**Fig. 4.** Electrochemical oscillation and single $H_2$ gas bubble detachment in 100 mM $H_2SO_4$. a, LSV curve with a scan rate of 100 mV $s^{-1}$. The dotted gray lines are approximate guidelines for distinguishing between the proton reduction reaction dominant region, the proton transport limited region and the water reduction reaction dominant region. b-d, Chronoamperometry measurements at –0.42 $V_{RHE}$ (b), –1.22 $V_{RHE}$ (c) and –1.82 $V_{RHE}$ (d). e-f, Periods and estimated detachment radius of single $H_2$ gas bubble obtained from electrochemical oscillation during chronoamperometry at –0.42 $V_{RHE}$ (e), –1.22 $V_{RHE}$ (f) and –1.82 $V_{RHE}$ (g). The estimated detachment radius of single $H_2$ gas bubble is determined assuming that all produced $H_2$ gas is captured by a single $H_2$ gas bubble.

addition of $Na^+$ cation (a more discussion on the effects of alkali metal cations will follow later). It is noteworthy that periodic single $H_2$ gas bubble formation and detachment can be observed even in the water reduction dominant region, indicating microbubble coalescence efficiency is still high enough, even with the additional formation of $OH^-$.

To gain further insights into the detachment of single $H_2$ gas bubbles in the 100 mM $H_2SO_4$ electrolyte, we conducted chronoamperometry measurements. At –0.42 $V_{RHE}$, where $H_2$ is produced through the proton reduction reaction with partial transport limitation, the HER current level and its oscillation features (period and estimated detachment radius) remained stable over 50 consecutive cycles. However, at –1.22 $V_{RHE}$, the HER current level decreased during the initial few oscillation cycles, alongside with a reduction in $H_2$ gas bubble detachment radius (Fig. 4c and 4f). The HER current observed at this potential (–0.18 mA) was higher than the $I_{trans}$ in 100 mM $H_2SO_4$ (–0.14 mA, derived from Eq. (2)), indicating that the thermal Marangoni effect becomes significant under these conditions. This phenomenon explains the observed reduction in $H_2$ gas bubble detachment radius alongside the decreased HER current during the initial oscillation cycles. With increasing overpotential, a longer stabilization time was required to achieve stabilization, which reflects the timescale needed for establishing a stable ion concentration field. Among convection, diffusion and migration, we believe that migration of the proton plays a critical role in determining this stabilization period. This hypothesis is supported by the observation that no such stabilization period is observed upon the addition of a supporting electrolyte which serves to inhibit proton migration (Supplementary Figure 7). After achieving stabilization, we analyzed the electrochemical oscillation and obtain the average values of the periods and the estimated detachment radius of single $H_2$ gas bubble at each potential. These values were consistent with those obtained from the electrochemical oscillation analysis of the LSV curve (Supplementary Figure 5), indicating that the scan rate of 100 mV $s^{-1}$ was sufficiently slow to capture the features of the stabilized ion concentration field.

As shown in Supplementary Figure 5, the oscillation period increased

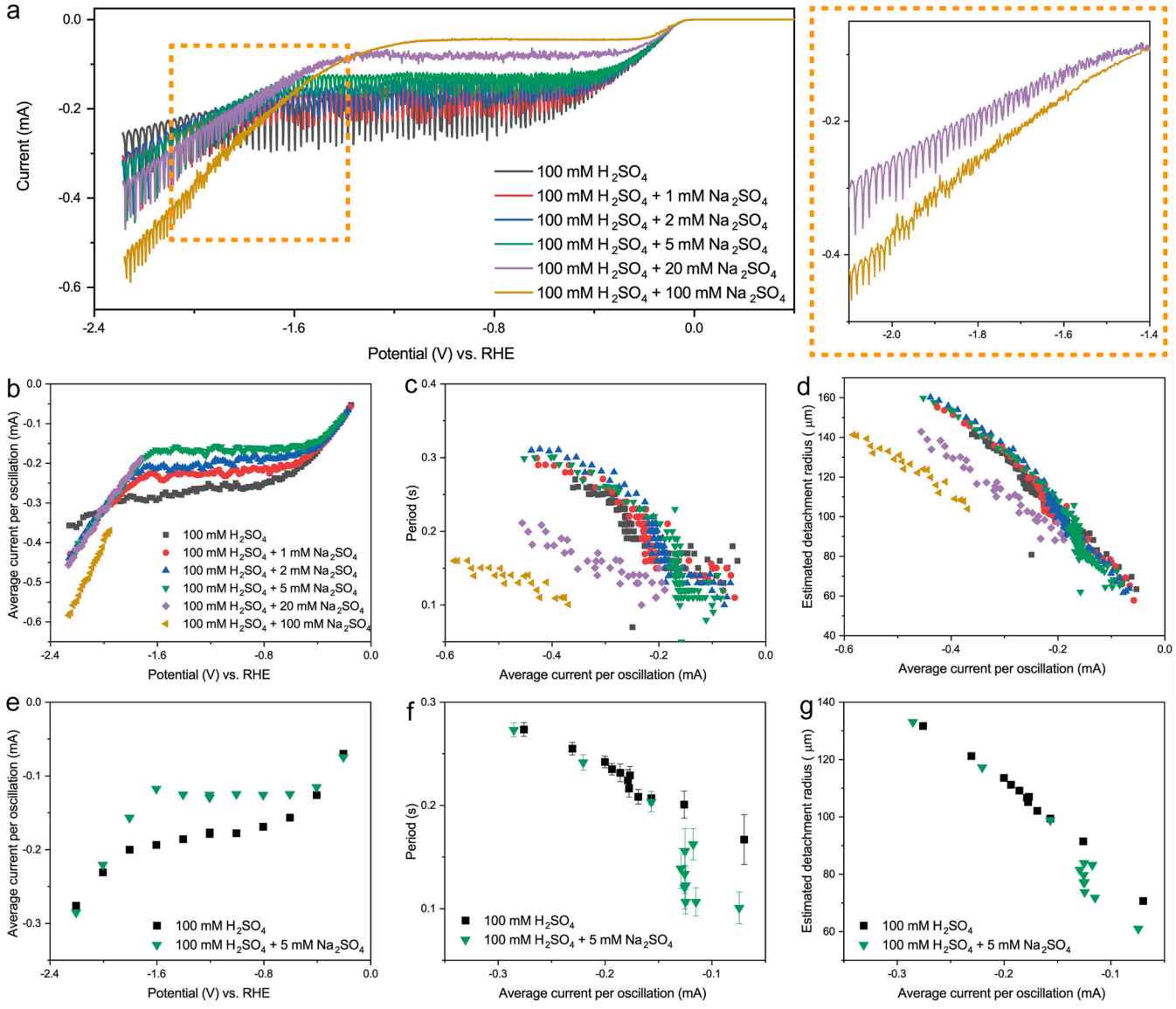


**Fig. 5.** $Na^+$ cation concentration effects on $H_2$ gas bubble evolution in 100 mM $H_2SO_4$. a, LSV curves with $Na_2SO_4$ at various concentrations measured at a scan rate of 100 mV $s^{-1}$. Orange dotted box shows enlarged graph focusing on the electrolytes with 20 and 100 mM $Na_2SO_4$ added. b-d, Average current (b), period (c) and estimated detachment radius (d) values obtained from the electrochemical oscillation in LSV curves in Fig. 5a. e-f, Average current (e), period (f) and estimated detachment radius (g) values obtained from the electrochemical oscillation in chronoamperometry (Supplementary Figure 7). The estimated detachment radius of a single $H_2$ gas bubble is determined assuming that all produced $H_2$ gas is captured by a single $H_2$ gas bubble.

with increasing overpotential or *I*, which is different from the v-shaped curves obtained at higher concentrations. Interestingly, no abrupt transitions in the period and estimated detachment radius graphs were observed at around –1.6 $V_{RHE}$, where a drastic local pH change was expected, and thus drastic change in ion concentration field, due to additional $OH^-$ formation from the water reduction reaction. This phenomenon might be attributed to the relatively small contribution of the solutal Marangoni effect and a relatively large contribution of thermal Marangoni effect in such a low concentration electrolyte.

### 3.2. Effect of alkali metal cation and bulk pH on $H_2$ gas bubble behaviour

To investigate the effect of alkali metal cations in the electrolyte on $H_2$ gas bubble behaviour, we added $Na_2SO_4$ as a supporting electrolyte to 100 mM $H_2SO_4$, keeping the $H_2SO_4$ concentration constant to minimize bulk pH changes. As shown in Fig. 5a, the onset of HER from the proton reduction reaction remains largely unchanged with the addition of $Na_2SO_4$. However, at more negative potentials, the HER current in the proton transport-limited region decreases with increasing $Na_2SO_4$ concentration (as also seen from the average *I* values at Fig. 5b), and the activity of water reduction reaction increases with increasing $Na_2SO_4$ concentration. These observed cation effects on HER currents are consistent with previous literature [37–41]. The decreasing diffusion-limited current in the proton transport-limited region with $Na_2SO_4$ addition clearly indicates that the migration of protons plays a substantial role in proton transport under our experimental conditions.

All electrolytes containing $Na_2SO_4$ exhibit random fluctuation at low HER current, with periodic oscillations becoming observable at high HER current. This occurrence suggests that microbubble coalescence is inhibited at low HER current, requiring a higher HER current to form a single $H_2$ gas bubble, as exemplified in Fig. 1b-d. To quantitatively study the coalescence efficiency of microbubbles, we compared the onset of the periodic oscillation, where single $H_2$ gas bubbles start to form (Supplementary Figure 6). This analysis confirms a clear positive correlation between the added $Na_2SO_4$ concentration and the onset HER current for periodic oscillation. Since sulfate anions exhibit the highest coalescence efficiency among all the anions we tested, ensuring the formation of single $H_2$ gas bubble in $H_2SO_4$ across all sulfate concentrations, we conclude that the higher concentration of $Na^+$ cations in the electrolyte lowers the coalescence efficiency of electrochemically generated $H_2$ microbubbles. The significant suppression of HER current oscillation/fluctuation at low HER currents with high $Na_2SO_4$ concentrations (e.g., 100 mM) might also be related to changes in gas bubble nucleation as well as microbubble coalescence efficiency. Considering that $H_2$ gas bubble nucleation requires approximately a 200-fold supersaturation [42], only a limited number of nucleation sites are expected on the microelectrode under low HER current conditions. Further research is necessary to fully understand the impact of high-concentration supporting electrolytes on gas bubble nucleation.

For small $Na_2SO_4$ additions ($\leq$ 5 mM), single $H_2$ gas bubble detachment is facilitated in the proton reduction reaction dominant region but has little effect on single $H_2$ gas bubble detachment in the water reduction reaction dominant region (Fig. 5c, d). This trend is more clearly seen in the data obtained through chronoamperometry (Fig. 5e-g and Supplementary Figure 7). According to Eq. (2), $I_{trans}$ for 100 mM $H_2SO_4$ is around –0.14 mA, which is similar to the proton transport-limited current. Therefore, in the proton reduction dominant region, the solutal Marangoni effect is dominant, and facile $H_2$ gas bubble detachment by adding $Na_2SO_4$ can be rationalized by the reduced sulfate anion concentration gradient field due to the enhanced cation migration in the mass transport boundary layer. Notably, adding only a few mM $Na^+$ cation is sufficient to alter the anion concentration gradient and resultant $H_2$ gas bubble detachment. On the other hand, in the water reduction region, the thermal Marangoni effect is dominant, similar $H_2$ gas bubble detachment can be rationalized by considering a small amount of $Na_2SO_4$, which does not substantially change the electrolyte conductivity to affect temperature gradient. With introduction of 5 mM $Na_2SO_4$, both period and detachment radius values exhibit an abrupt change at similar *I* in the proton transport limited region, which cannot be solely explained by variations in the Marangoni effect due to changes in *I*.

Furthermore, with a higher concentration of $Na_2SO_4$ ($\geq$ 20 mM), a faster detachment of single $H_2$ gas bubble with smaller sizes can be observed (Fig. 5c and 5d). It is notable that single $H_2$ gas bubbles only start to form in the regions where the HER current is large enough for the thermal Marangoni effect to dominate. Therefore, the more facile detachment of a single $H_2$ gas bubble with higher $Na_2SO_4$ concentration is likely due to the reduced thermal Marangoni force resulting from increased electrolyte conductivity with higher concentration of the supporting electrolyte.

We studied whether similar effects were observed for different types of alkali metal cations. We prepared 100 mM $H_2SO_4$ with 2 mM $Li_2SO_4$ ($\sigma_C$: 3.13 $mN\ m^{-1}/mol\ L^{-1}$), $Na_2SO_4$ ($\sigma_C$: 2.77$mN\ m^{-1}/mol\ L^{-1}$), $K_2SO_4$ ($\sigma_C$: 2.57 $mN\ m^{-1}/mol\ L^{-1}$) and $Cs_2SO_4$ ($\sigma_C$: 3.02 $mN\ m^{-1}/mol\ L^{-1}$) as supporting electrolytes [43] and analyzed their electrochemical oscillation patterns (Supplementary Figure 8). Similar to the case of $Na_2SO_4$ addition, enhanced single $H_2$ gas bubble detachment is observed in the proton reduction reaction dominant region in all electrolytes containing additional supporting electrolyte. Notably, we did not observe any remarkable differences in period and estimated detachment radius between different types of alkali metal cations of supporting electrolyte. This suggests that the effect of adding alkali metal cations is not specific, but rather related to the general effect it has on the corresponding anion concentration gradient.

Finally, we studied the effect of bulk pH on $H_2$ gas bubble evolution. Fig. 6a shows LSV curves obtained from various electrolytes with different bulk pH values while maintaining constant anion concentration. As the pH value increases from ca. 1 to 4, achieved by decreasing the $H_2SO_4$ concentration, the proton transport-limited current drastically decreases due to the lowered proton concentration and migration (Fig. 6b). In terms of $H_2$ gas bubble evolution, no periodic oscillation is observed in electrolytes with pH values higher than 1.7 (corresponding to 10 mM $H_2SO_4$ with 90 mM $Na_2SO_4$). This trend of microbubble coalescence inhibition with the addition of $Na^+$ cation is in line with the conclusion drawn from previous experiments: higher concentrations of $Na^+$ cations in the electrolyte lead to lower microbubble coalescence efficiency. However, it is noteworthy that the onset HER current of single $H_2$ gas bubble formation increased as the bulk pH of the electrolyte was increased.

For example, no single $H_2$ gas bubble formation is observed until –0.5 mA in 100 mM $Na_2SO_4$ electrolyte, whereas single $H_2$ gas bubbles start to form around –0.3 mA in 100 mM $H_2SO_4$ with 100 mM $Na_2SO_4$ electrolyte. Although these two electrolytes have the same bulk concentration of $Na^+$ cation, bulk pH values are different. Considering the more negative surface charge at higher bulk pH electrolyte at a given potential (on the RHE scale) as a result of higher potential of zero charge of platinum [44], the local concentration of $Na^+$ cation would be higher in the electrolyte of higher bulk pH [38,39]. This likely explains the more pronounced inhibition of microbubble coalescence in higher pH electrolytes. In alignment with this observation, all LSV curves obtained from neutral and alkaline electrolytes exhibit only small fluctuating HER current without periodic oscillation within the measured potential range (Fig. 6c).

## 4. General discussion and conclusion

In this study, we have demonstrated the effective control of the coalescence of electrochemically generated $H_2$ microbubbles by altering the composition and concentration of electrolytes. These results seem, at least partly, consistent with previous studies on air bubbles, where coalescence of air bubbles is inhibited under specific combinations of

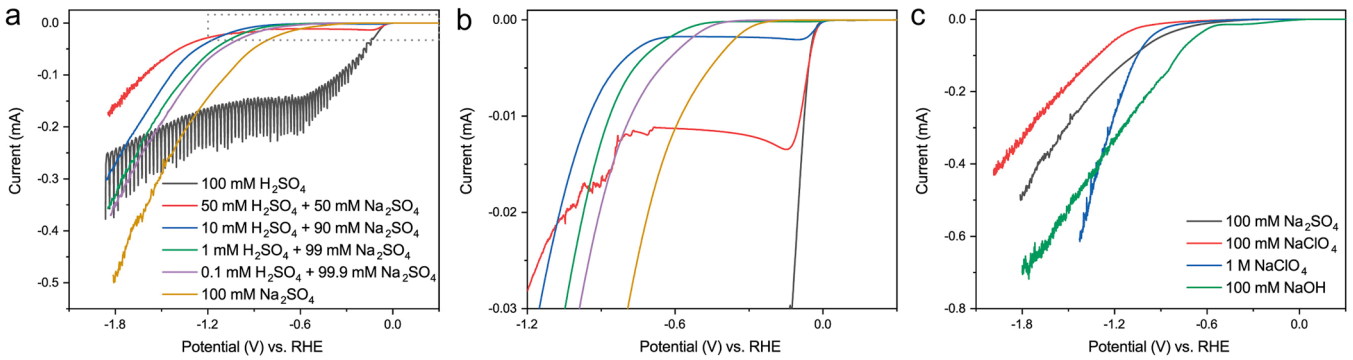


**Fig. 6.** Bulk pH effects on $H_2$ gas bubble evolution. a, LSV curves from sulfate-based electrolytes with various pH values. b, Enlarged plot of the gray dashed box in Fig. 6a. c, LSV curves from neutral and alkaline electrolytes. Scan rate: 100 mV $s^{-1}$.

dissolved ions in an electrolyte once a critical threshold is exceeded [45,46]. Although the exact mechanism responsible for the specific ion effects on inhibiting air bubble coalescence is not yet established, numerous studies have suggested that the inhibitory effect of these electrolytes is associated with the slowing down of the thinning dynamics of liquid film between bubbles [47,48]. This is influenced by factors such as colliding speed and the particular arrangement of ions at the bubble/electrolyte interface [48,49]. Craig *et al.*'s empirical classification of ions categorizes an electrolyte with an α cation and an α anion (αα) or a ββ combination as an electrolyte that inhibits air bubble coalescence, whereas αβ or βα combinations have no inhibiting effect [50]. According to this empirical classification, related to the Hofmeister series, all alkali metal cations are classified as α cations, while the proton is classified as a β cation. Regarding anions, $SO_4^{2-}$, $Cl^-$, $NO_3^-$, and $OH^-$ are classified as α anions, while $ClO_4^-$ is classified as a β anion. Based on these empirical observations, one can predict whether air bubble coalescence will be inhibited under the given concentration and composition of the electrolyte.

For example, $NaClO_4$ (αβ) might be expected to exhibit no inhibition of gas bubble coalescence, resulting in the facile formation of single $H_2$ gas bubbles and periodic oscillation during the HER. However, the LSV results for $NaClO_4$ show small fluctuating HER current without periodic oscillation, indicating inhibited coalescence of $H_2$ microbubbles under the measured condition (Fig. 6c). Therefore, to explain observed trends in $H_2$ microbubbles coalescence during electrochemical HER, the unique characteristics of electrochemically generated gas bubbles need to be considered. During the electrochemical HER, microbubbles are generated near to the surface of the electrode where the electrochemical reaction takes place. Consequently, electrochemically generated microbubbles are influenced by the local ion environment, which is strongly dependent on local mass transport and surface electrochemical reactions. During the proton reduction reaction in acidic electrolytes, local ion concentrations decrease as the HER current increases due to proton consumption at the surface, which might explain the abrupt change in gas bubble evolution in acidic electrolytes around the onset HER current of periodic oscillation. For the water reduction reaction, local ion composition can also be altered compared to bulk properties. As the HER current increases, more $OH^-$ anions are generated on the surface, making the local ion composition more similar to MOH (M: alkali metal cation), which corresponds to an αα electrolyte according to empirical classification. This might explain why the coalescence of electrochemically generated $H_2$ microbubbles is severely inhibited in all neutral and alkaline electrolytes, regardless of bulk electrolyte composition and concentration.

When the coalescence efficiency is sufficiently high, we observed periodic formation and detachment of single $H_2$ gas bubbles, which can be controlled by altering the composition and concentration of electrolytes. To rationalize the detachment of single $H_2$ gas bubbles, a detailed force equilibrium should be considered. Several forces contribute to the behaviour of the single $H_2$ gas bubble, including buoyance force, capillary force if the single gas bubble is in contact with electrode [19], force due to the coalescence with other microbubbles if single gas bubble is sitting on a microbubble carpet[28], electrical force [26], and Marangoni forces (both thermal and solutal)[30]. In addition to solutal Marangoni force, the electrical force might explain the observed electrolyte-dependent detachment of single $H_2$ gas bubbles, as the surface charge of the gas bubble can be altered by electrolyte composition and concentration, primarily by the pH of the electrolyte [51,52]. Because the electrical force is proportional to the surface charge of the gas bubble and applied potential, a constant electrical force is expected during the chronoamperometry measurements at a fixed potential. However, the observed data in Fig. 4 (where the detachment size of single $H_2$ gas bubble changes during chronoamperometry at a fixed potential) directly indicate that considering only electrical force is insufficient to explain the detachment of electrochemically generated single $H_2$ gas bubble. Therefore, we believe that the proposed model, which considers a change in (the type of) Marangoni force, is a more appropriate model under our experimental conditions, capable of qualitatively explaining all variations in single $H_2$ gas bubble detachment we observed.

To summarize, in this work we have comprehensively investigated the evolution of $H_2$ gas bubbles in various electrolytes and confirmed that a simple model based on two competing Marangoni effects (solutal and thermal) effectively explains single $H_2$ gas bubble behaviour during the HER on a Pt microelectrode. In acidic electrolytes, without alkali metal cations, the microbubble coalescence efficiency follows the Hofmeister series of anions, which determines the onset of single $H_2$ gas bubble formation. The detachment size and period of a single $H_2$ gas bubble follow well the considerations of the Marangoni effects. In the low HER current region, the dominant factor is the solutal Marangoni effect induced by anion concentration gradients, while in the high HER current region, the controlling factor shifts to the thermal Marangoni effect induced by a temperature gradient. The addition of alkali metal cations in acidic electrolytes reduces the microbubble coalescence efficiency and enhances the detachment of a single $H_2$ gas bubble by altering ion distribution and/or electrolyte conductivity. In neutral and alkaline conditions, only multiple $H_2$ gas bubble detachment is observed without the formation of single $H_2$ gas bubbles up to –0.5 mA (equivalent to –6.4 A $cm^{-2}$ of geometric current density). This is attributed to the high local concentration of alkali metal cations and $OH^-$ near the Pt surface. The findings presented in this work provide valuable insights for understanding and designing electrolytes to manipulate $H_2$ gas bubble evolution during the HER.

## Data availability

All relevant data generated and analysed during this study are included in this article and its Supplementary Information.

Data for the main figures are available in Zenodo (10.5281/zenodo.10355728)

Supplementary materials

Supplementary material associated with this article can be found, in the online version.

## Declaration of competing interest

The authors declare that they have no known competing financial interests or personal relationships that could have appeared to influence the work reported in this paper.

## Acknowledgements

S.P. acknowledges the support by Basic Science Research Program through the National Research Foundation of Korea (NRF) funded by the Ministry of Education (2021R1A6A3A14039678). D.L and D.K. thank the Dutch Research Council (NWO) for funding via the Max Planck Center Twente and via the Advanced Research Center Chemical Building Blocks Consortium (ARC-CBBC).

## Supplementary materials

Supplementary material associated with this article can be found, in the online version, at doi:10.1016/j.electacta.2024.144084.

## References

[1] J.A. Turner, Sustainable hydrogen production, Science (1979) 305 (2004) 972–974.
[2] S. van Renssen, The hydrogen solution? Nat. Clim. Chang. 10 (2020) 799–801.
[3] A. Kovač, M. Paranos, D. Marciuš, Hydrogen in energy transition: A review, Int. J. Hydrogen Energy 46 (2021) 10016–10035.
[4] A.J. Shih, M.C.O. Monteiro, F. Dattila, D. Pavesi, M. Philips, A.H.M. da Silva, R. E. Vos, K. Ojha, S. Park, O. van der Heijden, G. Marcandalli, A. Goyal, M. Villalba, X. Chen, G.T.K.K. Gunasooriya, I. McCrum, R. Mom, N. López, M.T.M. Koper, Water electrolysis, Nature Reviews Methods Primers 2 (2022) 84.
[5] M. Chatenet, B.G. Pollet, D.R. Dekel, F. Dionigi, J. Deseure, P. Millet, R.D. Braatz, M.Z. Bazant, M. Eikerling, I. Staffell, P. Balcombe, Y. Shao-Horn, H. Schäfer, Water electrolysis: from textbook knowledge to the latest scientific strategies and industrial developments, Chem. Soc. Rev. 51 (2022) 4583–4762.
[6] National Institute of Standards and Technology, IUPAC-NIST solubility database, version 1.1. NIST standard reference database 106 (2012).
[7] M.J. Tham, R.D. Walker, K.E. Gubbins, Diffusion of oxygen and hydrogen in aqueous potassium hydroxide solutions, J. Phys. Chem. 74 (1970) 1747–1751.
[8] X. Zhao, H. Ren, L. Luo, Gas Bubbles in Electrochemical Gas Evolution Reactions, Langmuir 35 (2019) 5392–5408.
[9] A. Angulo, P. van der Linde, H. Gardeniers, M. Modestino, D.Fernández Rivas, Influence of Bubbles on the Energy Conversion Efficiency of Electrochemical Reactors, Joule 4 (2020) 555–579.
[10] H. Vogt, R.J. Balzer, The bubble coverage of gas-evolving electrodes in stagnant electrolytes, Electrochim. Acta 50 (2005) 2073–2079.
[11] J.R. Lake, Á.M. Soto, K.K. Varanasi, Impact of Bubbles on Electrochemically Active Surface Area of Microtextured Gas-Evolving Electrodes, Langmuir 38 (2022) 3276–3283.
[12] C. Gabrielli, F. Huet, R.P. Nogueira, Fluctuations of concentration overpotential generated at gas-evolving electrodes, Electrochim. Acta 50 (2005) 3726–3736.
[13] J. Dukovic, C.W. Tobias, The Influence of Attached Bubbles on Potential Drop and Current Distribution at Gas-Evolving Electrodes, J. Electrochem. Soc. 134 (1987) 331–343.
[14] H. Vogt, The voidage problem in gas-electrolyte dispersions, J. Appl. Electrochem. 17 (1987) 419–426.
[15] M.G. Fouad, G.H. Sedahmed, Mass transfer at horizontal gas-evolving electrodes, Electrochim. Acta 18 (1973) 55–58.
[16] S. Yuan, C. Zhao, X. Cai, L. An, S. Shen, X. Yan, J. Zhang, Bubble evolution and transport in PEM water electrolysis: Mechanism, impact, and management, Prog. Energy Combust. Sci. 96 (2023) 101075.
[17] G.F. Swiegers, R.N.L. Terrett, G. Tsekouras, T. Tsuzuki, R.J. Pace, R. Stranger, The prospects of developing a highly energy-efficient water electrolyser by eliminating or mitigating bubble effects, Sustain. Energy Fuels 5 (2021) 1280–1310.
[18] H.N. Oguz, A. Prosperetti, Dynamics of bubble growth and detachment from a needle, J. Fluid Mech. 257 (1993) 111–145.
[19] P. Lv, H. Le The, J. Eijkel, A. Van Den Berg, X. Zhang, D. Lohse, Growth and Detachment of Oxygen Bubbles Induced by Gold-Catalyzed Decomposition of Hydrogen Peroxide, J. Phys. Chem. C 121 (2017) 20769–20776.
[20] P. Van Der Linde, P. Peñas-López, Á.Moreno Soto, D. Van Der Meer, D. Lohse, H. Gardeniers, D.Fernández Rivas, Gas bubble evolution on microstructured silicon substrates, Energy Environ. Sci. 11 (2018) 3452–3462.
[21] P. Lv, P. Peñas, H. Le The, J. Eijkel, A. Van Den Berg, X. Zhang, D. Lohse, Self-Propelled Detachment upon Coalescence of Surface Bubbles, Phys. Rev. Lett. 127 (2021) 235501.
[22] R. Iwata, L. Zhang, Z. Lu, S. Gong, J. Du, E.N. Wang, How Coalescing Bubbles Depart from a Wall, Langmuir 38 (2022) 4371–4377.
[23] S.D. Lubetkin, The fundamentals of bubble evolution, Chem. Soc. Rev. 24 (1995) 243–250.
[24] S. Lubetkin, The motion of electrolytic gas bubbles near electrodes, Electrochim. Acta 48 (2002) 357–375.
[25] X. Yang, D. Baczyzmalski, C. Cierpka, G. Mutschke, K. Eckert, Marangoni convection at electrogenerated hydrogen bubbles, Phys. Chem. Chem. Phys. 20 (2018) 11542–11548.
[26] A. Bashkatov, S.S. Hossain, X. Yang, G. Mutschke, K. Eckert, Oscillating Hydrogen Bubbles at Pt Microelectrodes, Phys. Rev. Lett. 123 (2019) 214503.
[27] J. Massing, G. Mutschke, D. Baczyzmalski, S.S. Hossain, X. Yang, K. Eckert, C. Cierpka, Thermocapillary convection during hydrogen evolution at microelectrodes, Electrochim. Acta 297 (2019) 929–940.
[28] S.S. Hossain, A. Bashkatov, X. Yang, G. Mutschke, K. Eckert, Force balance of hydrogen bubbles growing and oscillating on a microelectrode, Phys. Rev. E 106 (2022) 035105.
[29] A.M. Meulenbroek, A.W. Vreman, N.G. Deen, Competing Marangoni effects form a stagnant cap on the interface of a hydrogen bubble attached to a microelectrode, Electrochim. Acta 385 (2021) 138298.
[30] S. Park, L. Liu, Ç. Demirkır, O. van der Heijden, D. Lohse, D. Krug, M.T.M. Koper, Solutal Marangoni effect determines bubble dynamics during electrocatalytic hydrogen evolution, Nat. Chem. 15 (2023) 1532–1540.
[31] X. Yang, F. Karnbach, M. Uhlemann, S. Odenbach, K. Eckert, Dynamics of Single Hydrogen Bubbles at a Platinum Microelectrode, Langmuir 31 (2015) 8184–8193.
[32] P.K. Weissenborn, R.J. Pugh, Surface Tension of Aqueous Solutions of Electrolytes: Relationship with Ion Hydration, Oxygen Solubility, and Bubble Coalescence, J. Colloid. Interface Sci. 184 (1996) 550–563.
[33] J.P. Guthrie, Hydrolysis of esters of oxy acids: $pK_a$ values for strong acids; Brønsted relationship for attack of water at methyl; free energies of hydrolysis of esters of oxy acids; and a linear relationship between free energy of hydrolysis and $pK_a$ holding over a range of 20 pK units, Can. J. Chem. 56 (1978) 2342–2354.
[34] K.P. Gregory, G.R. Elliott, H. Robertson, A. Kumar, E.J. Wanless, G.B. Webber, V.S. J. Craig, G.G. Andersson, A.J. Page, Understanding specific ion effects and the Hofmeister series, Phys. Chem. Chem. Phys. 24 (2022) 12682–12718.
[35] L.F. Nims, The First Dissociation Constant of Phosphoric Acid from 0 to 50°, J. Am. Chem. Soc. 56 (1934) 1110–1112.
[36] M.N. Jackson, O. Jung, H.C. Lamotte, Y. Surendranath, Donor-Dependent Promotion of Interfacial Proton-Coupled Electron Transfer in Aqueous Electrocatalysis, ACS Catal. 9 (2019) 3737–3743.
[37] B. Huang, R.R. Rao, S. You, K. Hpone Myint, Y. Song, Y. Wang, W. Ding, L. Giordano, Y. Zhang, T. Wang, S. Muy, Y. Katayama, J.C. Grossman, A.P. Willard, K. Xu, Y. Jiang, Y. Shao-Horn, Cation- and pH-Dependent Hydrogen Evolution and Oxidation Reaction Kinetics, JACS Au 1 (2021) 1674–1687.
[38] M.C.O. Monteiro, A. Goyal, P. Moerland, M.T.M. Koper, Understanding Cation Trends for Hydrogen Evolution on Platinum and Gold Electrodes in Alkaline Media, ACS Catal. 11 (2021) 14328–14335.
[39] A. Goyal, M.T.M. Koper, The Interrelated Effect of Cations and Electrolyte pH on the Hydrogen Evolution Reaction on Gold Electrodes in Alkaline Media, Angew. Chem. Int. Ed. 60 (2021) 13452–13462.
[40] A.H. Shah, Z. Zhang, Z. Huang, S. Wang, G. Zhong, C. Wan, A.N. Alexandrova, Y. Huang, X. Duan, The role of alkali metal cations and platinum-surface hydroxyl in the alkaline hydrogen evolution reaction, Nat. Catal. 5 (2022) 923–933.
[41] S. Xue, B. Garlyyev, S. Watzele, Y. Liang, J. Fichtner, M.D. Pohl, A.S. Bandarenka, Influence of Alkali Metal Cations on the Hydrogen Evolution Reaction Activity of Pt, Ir, Au, and Ag Electrodes in Alkaline Electrolytes, ChemElectroChem 5 (2018) 2326–2329.
[42] L. Luo, H.S. White, Electrogeneration of Single Nanobubbles at Sub-50-nm-Radius Platinum Nanodisk Electrodes, Langmuir 29 (2013) 11169–11175.
[43] L.M. Pegram, M.T. Record, Hofmeister Salt Effects on Surface Tension Arise from Partitioning of Anions and Cations between Bulk Water and the Air−Water Interface, J. Phys. Chem. B 111 (2007) 5411–5417.

[44] R. Rizo, E. Sitta, E. Herrero, V. Climent, J.M. Feliu, Towards the understanding of the interfacial pH scale at Pt(1 1 1) electrodes, Electrochim. Acta 162 (2015) 138–145.
[45] G. Marrucci, L. Nicodemo, Coalescence of gas bubbles in aqueous solutions of inorganic electrolytes, Chem. Eng. Sci. 22 (1967) 1257–1265.
[46] R.R. Lessard, S.A. Zieminski, Bubble Coalescence and Gas Transfer in Aqueous Electrolytic Solutions, Ind. Eng. Chem. Fundamen. 10 (1971) 260–269.
[47] V.S.J. Craig, Do hydration forces play a role in thin film drainage and rupture observed in electrolyte solutions? Curr. Opin. Colloid. Interface Sci. 16 (2011) 597–600.
[48] B. Liu, R. Manica, Q. Liu, Z. Xu, E. Klaseboer, Q. Yang, Nanoscale Transport during Liquid Film Thinning Inhibits Bubble Coalescing Behavior in Electrolyte Solutions, Phys. Rev. Lett. 131 (2023) 104003.
[49] V.S.J. Craig, C.L. Henry, Specific Ion Effects at the Air–Water Interface: Experimental Studies, in: Specific Ion Effects, World Scientific (2009) 191–214.
[50] V.S.J. Craig, B.W. Ninham, R.M. Pashley, The effect of electrolytes on bubble coalescence in water, J. Phys. Chem. 97 (1993) 10192–10197.
[51] N.P. Brandon, G.H. Kelsall, S. Levine, A.L. Smith, Interfacial electrical properties of electrogenerated bubbles, J. Appl. Electrochem. 15 (1985) 485–493.
[52] M. Takahashi, ζ Potential of Microbubbles in Aqueous Solutions: Electrical Properties of the Gas−Water Interface, J. Phys. Chem. B. 109 (2005) 21858–21864.